Available online at www.sciencedirect.com

SciVerse ScienceDirect

Advances in Space Research 52 (2013) 251–261

ADVANCES IN SPACE RESEARCH (a COSPAR publication)

www.elsevier.com/locate/asr

The lunar dust pendulum

Michael R. Collier [a,c,*], William M. Farrell [a,c], Timothy J. Stubbs [a,b,c]

[a] NASA/Goddard Space Flight Center, Code 695, Greenbelt, MD 20771, USA
[b] Center for Research and Exploration in Space Science and Technology, University of Maryland, Baltimore County, MD 21250, USA
[c] NASA's Lunar Science Institute, NASA Ames Research Center, Moffett Field, CA 94035, USA

Available online 13 October 2012

Abstract

An analytic model for the motion of a positively charged lunar dust grain in the presence of a shadowed crater at a negative potential in vacuum is presented. It is shown that the dust grain executes oscillatory trajectories, and an expression is derived for the period of oscillation. Simulations used to verify the analytic expression also show that because the trajectories are unstable, dust grains are either ejected from the crater's vicinity or deposited into the crater forming "dust ponds." The model also applies to other airless bodies in the solar system, such as asteroids, and predicts that under certain conditions, particularly near lunar sunset, oscillating dust "canopies" or "swarms" will form over negatively charged craters.
Published by Elsevier Ltd. on behalf of COSPAR.

Keywords: Lunar dust; Electrostatic transport; Lunar surface potential

1. Introduction

The lunar surface is exposed to solar irradiation and the ambient plasma environment, usually the solar wind. Because the Moon has only a tenuous exosphere, charged particles as well as photons are absorbed by the regolith causing it to acquire a potential, either positive or negative, that enforces current balance [e.g., Collier et al., 2011a]. Generally, on the dayside the photoemission of electrons from the lunar surface charges it positive, while on the nightside the large plasma electron thermal speed produces a negative potential (Manka, 1973; Whipple, 1981; Fenner et al., 1973), although more complex situations can occur, for example when the Moon is in the terrestrial plasma sheet [e.g., Poppe et al., 2011 and references therein; Poppe and Horányi, 2010]. Similarly shadowed regions and, in particular, shadowed craters can have a negative potential with respect to the surrounding lunar regolith in sunlight, especially near the terminator regions (Stubbs et al., 2010; Borisov and Mall, 2006).

In particular, near the sunset terminator, there exists an offset between the optical shadow and the plasma wake. Consequently, the regolith experiences an unusually tenuous plasma (which results in a large Debye length) and sunlight simultaneously, conditions conducive to producing negatively charged shadowed craters (Stubbs et al., 2010).

Among the effects of the frequently complex lunar electric field configuration is the electrostatic transport of charged lunar dust grains (Singer and Walker, 1962). Previous work describing the transport of charged lunar dust in its electrostatic environment concentrated on the vertical component of motion. For example, Stubbs et al. (2006) considered dust lofting in which charged lunar dust grains are accelerated vertically through the plasma sheath whereupon they follow ballistic trajectories. Laboratory experiments have been successful levitating large (e.g., 10 μ) charged dust grains [e.g., Wang et al., 2009; Sickafoose et al., 2002], with required electric fields of about 50 V/cm.

However, lunar electric fields, particularly near the terminator and resulting from topography that is not level,

* Corresponding author at: NASA/Goddard Space Flight Center, Code 695, Greenbelt, Maryland 20771, USA. Tel.: +1 301 286 5256; fax: +1 301 614 6015.
E-mail addresses: michael.r.collier@nasa.gov (M.R. Collier), william.m.farrell@nasa.gov (W.M. Farrell), timothy.j.stubbs@nasa.gov (T.J. Stubbs).

0273-1177/$36.00 Published by Elsevier Ltd. on behalf of COSPAR.
http://dx.doi.org/10.1016/j.asr.2012.09.044

will not be confined to the vertical direction and will usually have a significant horizontal component. For example, one interpretation of the Apollo 17 Lunar Ejecta and Meteorites (LEAM) experiment's observation of highly charged dust moving at ≈100 m/s near the terminator is that dust is transported due to the complex electric fields in this region (Berg et al., 1976; Colwell et al., 2007; Farrell et al., 2007). (However see O'Brien (2011) for an alternative interpretation of the LEAM observations).

Colwell et al. (2005) in investigating dust transport on Eros did include horizontal transport (although not horizontal electric fields) and found oscillatory behavior in the vertical direction (see e.g. their Fig.5). They modeled charged dust dynamics in the dayside plasma environment of Eros and included both the horizontal and vertical transport in the photoelectron layer. In Colwell et al.'s approach, when a particle leaves the surface, the current due to photoelectrons from the surface sheath exceeds the current due to its own photoemission of electrons, such that it can attain a negative charge as it passes through the photoelectron layer. Thus a charged dust grain on the sunlit side traversing the photoelectric sheath sees variable currents over its trajectory so its charge is time-dependent.

We analyze the motion of a positively charged lunar dust grain in the presence of a shadowed crater at a negative potential in vacuum. Clearly the electric fields in the vicinity of shadowed craters will have significant components in the horizontal directions. We propose a model that includes both the horizontal and vertical motion of charged dust grains near shadowed craters. We show that the dust grains execute oscillatory trajectories and present an expression for the period of oscillation.

2. A shadowed crater model

Because shadowed regions tend to acquire a negative charge (Farrell et al., 2008; Stubbs et al., 2010; Zimmerman et al., 2011), and crater depths are characteristically significantly smaller than their radius [e.g., Hörz et al., 1991 and references therein], we approximate a shadowed lunar crater as a disk of radius a at a potential V_0 within an infinite plane at zero potential representing the unshadowed lunar regolith, as shown in Fig. 1. This condition would be most closely met near the lunar terminator region where the potential goes from positive on the dayside to negative on the nightside and would be induced by topographical effects – as illustrated by Fig. 3 of Farrell et al. (2007) in which elevated regions could be sunlit and neutral or slightly positively charged by photoemission, while floor regions would be unlit negatively charged. This is, of course, an idealized model that captures the physical essence of the problem and permits an analytic solution.

Although we present the model here as applicable to shadowed lunar craters, it could equally-well be applied to other airless bodies such as Mercury and some moons of the outer planets (and maybe even comets far from the sun [e.g., Mendis et al., 1981] and asteroids (Colwell et al., 2005) which also exhibit variable surface potentials). It may also be applied, for that matter, to objects that are not craters, for example, a rover tire lying flat on the regolith.

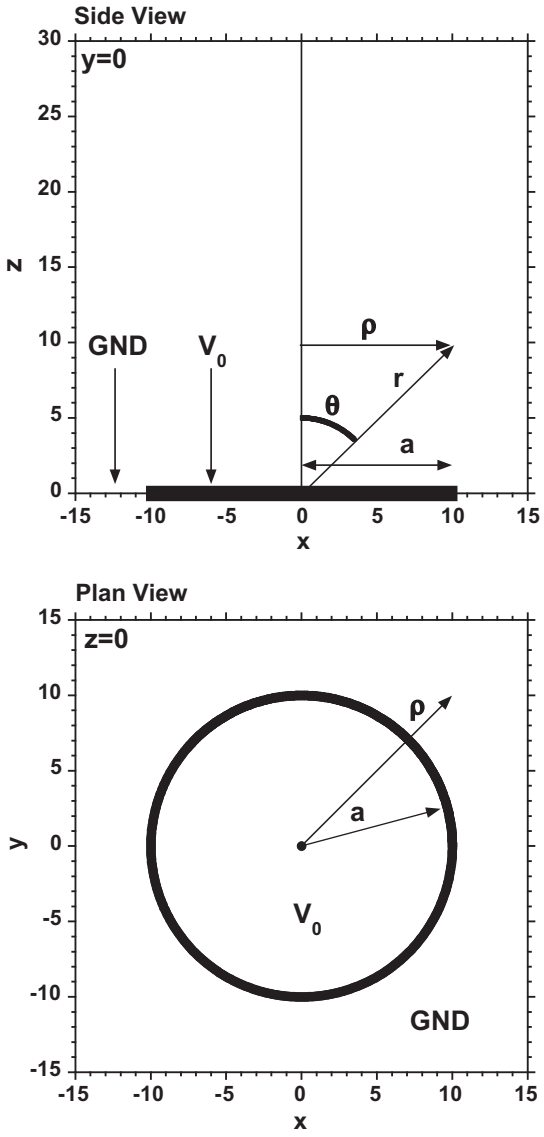

Fig. 1. The shadowed crater model assumes a disk of potential $\Phi = V_0$ at $z = 0$ when $\rho \leqslant a$ and $\Phi = 0$ at $z = 0$ when $\rho > a$. The Debye length is taken to be greater than the characteristic length scales.

Perhaps (even as far as surface topography goes) a crater is not necessary, for example, a shadowed region behind a boulder might suffice. Topography is particularly important because it can produce situations in which a part of the surface charges negative and another part remains neutral or positive; i.e., create large differential charging. So the situation analyzed here may actually occur, to some degree of approximation, quite frequently. Furthermore, surface composition and grain size will also locally affect charging processes. Note here that we also assume that the length scales of interest are less than the Debye length and correspondingly that the plasma is diffuse enough so that the

dust potentials are time-independent; that is, there is no appreciable change in the grain charge after it leaves the surface. Near the terminator, the Debye length can easily be of the order of ten meters. We also take the lunar surface potentials to be in steady-state. These conditions and the validity of the assumptions will be more fully addressed in Section 4.

3. Analytical Solution – general discussion

So, formally, then, we solve the problem shown in Fig. 1 where the crater potential $\Phi = V_0$ if $z = 0$ and $\rho \leqslant a$, while the potential $\Phi = 0$ if $z = 0$ and $\rho > a$, where z and ρ are in cylindrical coordinates so that $r^2 = \rho^2 + z^2$ where r is the distance from the crater center. Because the potential approaches zero infinitely far from the crater, we can expand the solution $\Phi(r,z)$ for the potential in spherical harmonics keeping only the $m = 0$ terms because the problem has azimuthal symmetry:

$$\Phi(r,z) = \sum_{n=0}^{\infty} \frac{B_n P_n(\cos\theta)}{r^{n+1}}. \tag{1}$$

In Eq. (1), B_n are the expansion coefficients and $P_n(\cos\theta)$ are the Legendre polynomials, the first few of which are:

$$P_0(\cos\theta) = 1, \tag{2a}$$

$$P_1(\cos\theta) = \cos\theta, \tag{2b}$$

$$P_2(\cos\theta) = \frac{1}{2}(3\cos^2\theta - 1), \tag{2c}$$

$$P_3(\cos\theta) = \frac{1}{2}(5\cos^3\theta - 3\cos\theta), \tag{2d}$$

and so on for higher orders [e.g., Abramowitz and Stegun, 1972].

Because $\theta = \pi/2$ (measured relative to the z-axis – i.e. at $z = 0$) defines the ground plane at $r = \rho > a$, the potential is zero there so that only the odd n terms contribute to the expansion. This is because the even n terms are non-zero at $\theta = \pi/2$ in Eq. (2a)–(2d) and their presence would violate the boundary conditions. Thus, an approximation which is good to the $n = 3$ octupole moment, which is non-zero, is

$$\Phi(r,z) = \frac{B_1 P_1(\cos\theta)}{r^2}. \tag{3}$$

That is, the potential configuration is, to first order (and second order), a dipole.

It is worth noting here that Eq. (3) is valid even for a non-circular crater. This is because the boundary conditions in the problem force the $m = \pm 1$ terms when $n = 1$ to zero, and because the quadrupole moment and higher terms become negligible a short distance from the source. Here m is the constant used for the azimuthal term when solving Laplace's equation by separation of variables. Thus, although we solve the problem analytically assuming a symmetric circular crater, the general results hold for a crater of arbitrary shape. The analytical treatment allows us to establish scaling relationships for the problem.

Although some may find it counter-intuitive that the physical situation described above produces a dipole potential configuration, this field configuration can be thought of as resulting from the presence of the ground plane which forces the otherwise monopole-like electric field lines from the charged crater to bend around and intersect normal to the surface for $\rho > a$, thereby forming a dipolar configuration.

It remains to determine the dipole moment B_1 which, dimensionally, is $[Ql]$ where Q is the charge and l is a characteristic length. Because the dimensionality of voltage $[V] = [Q/l/\epsilon_0]$ and the only length scale in the problem is a, we know that the dipole moment will scale as $\epsilon_0 V_0 a^2$.

It should be noted at this point that the problem as formulated here is a standard text book problem (Jackson, 1975) and has a closed-form solution:

$$\Phi(\rho,z) = \int_0^{\infty} V_0 a J_1(ka) J_0(k\rho)\exp\{-kz\}dk, \tag{4}$$

where J_0 and J_1 are the Bessel functions of order zero and one, respectively. So, we can simply expand $J_1(ka)$ as

$$J_1(ka) \approx \frac{ka}{2} - \frac{ka^3}{16}, \tag{5}$$

to deduce that the dipole moment is $V_0 a^2/2$.

Formally, if we expand $J_1(ka)$ as above but to first order, then the integral becomes

$$\Phi(\rho,z) = \int_0^{\infty} V_0 a \cdot \frac{ka}{2} \cdot J_0(k\rho)\exp\{-kz\}dk. \tag{6}$$

Since

$$k\exp\{-kz\} = -\frac{\partial}{\partial z}\exp\{-kz\}, \tag{7}$$

we can recast the integral as

$$\Phi(\rho,z) = -\frac{V_0 a^2}{2} \cdot \frac{\partial}{\partial z}\left[\int_0^{\infty} J_0(k\rho)\exp\{-kz\}dk\right]. \tag{8}$$

Using the identity

$$\frac{1}{\sqrt{\rho^2+z^2}} = \int_0^{\infty} \exp\{-kz\}J_0(k\rho)\,dk, \tag{9}$$

we get

$$\Phi(\rho,z) = \frac{V_0 a^2}{2} \cdot \frac{z}{[\rho^2+z^2]^{3/2}}. \tag{10}$$

Because we can write $r = \sqrt{\rho^2+z^2}$ and $z = r\cos\theta$ where r and θ are in spherical coordinates, this is equivalent to

$$\Phi(r,\theta) = \frac{V_0 a^2}{2} \cdot \frac{\cos\theta}{r^2}, \tag{11}$$

and we immediately identify this as the form for a dipole potential with a moment of $V_0 a^2/2$. Again, it should be noted that the dipole potential is valid for a shadowed area of any shape at distances much larger than the largest dimension of the area. For a more heuristic approach to determining the dipole moment, see the appendix.

3.1. Circular motion

As discussed by Jones (1995) charged particle, which in this context is a lunar dust grain, starting at rest on the zero potential, bisecting plane (i.e., the lunar surface) in a dipole potential will move along a semi-circular path. In reference to the left hand panel of Fig. 2 (where the particle is assumed to be at a distance $r = d$ from the crater center), if the dipole potential is given by Eq. (11) then the electric field in the radial direction, E_r, is simply given by

$$E_r = -\frac{\partial \Phi}{\partial r} = \frac{V_0 a^2 \cos\theta}{r^3}. \tag{12}$$

We will now show that this is exactly the electric field necessary to maintain the dust grain in circular motion. Circular motion requires that

$$\frac{mv^2}{r} = -qE_r = -\frac{qV_0 a^2 \cos\theta}{r^3}. \tag{13}$$

If the charged dust grain starts out at rest on the surface (or close to the surface with negligible velocity) which is at zero potential, the particle's total energy is zero. So, we can determine what mv^2/r is for the particle at any point (r, θ) using energy conservation:

$$\frac{mv^2}{2} + q\Phi(r,\theta) = 0. \tag{14}$$

In this scenario there is no initial velocity at the surface, since we are modeling a case where the electric force overcomes cohesion forces to get the grains moving (or a saltation mechanism) as opposed, for example, to a grain directly ejected by a micro-meteoroid. Multiplying by $2/r$, we get

$$\frac{mv^2}{r} = -\frac{2q\Phi(r,\theta)}{r} = -\frac{qV_0 a^2 \cos\theta}{r^3}. \tag{15}$$

Comparing with Eq. (13), this shows that the dipole field supplies exactly the necessary radial force to keep the dust grain in circular motion.

3.2. Analogy to gravitational pendulum

There exists a close correspondence between the behavior of a standard gravitational pendulum and the lunar dust pendulum described here. Fig. 2 shows both the lunar dust or electrostatic pendulum on the left and the gravitational pendulum, consisting of a mass m on a string on the right. In both cases, the "length" of the pendulum is d. In the case of the dust pendulum, this is the distance from the crater center, and in the case of the gravitational pendulum it is the length of the string.

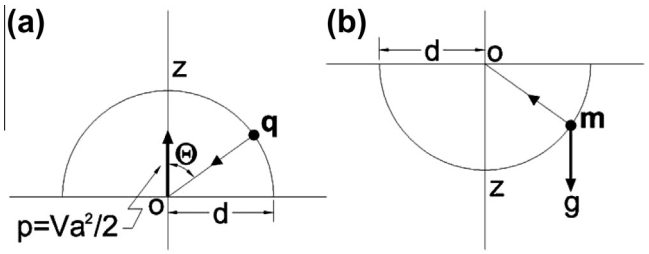

Fig. 2. (a) Electrostatic pendulum: the coordinate system used to show that in the presence of dipole moment $V_0 a^2/2$ a charged dust grain will execute circular motion. Note that the potential increases with increasing z. (b) Gravitational pendulum: the analogy between the dust pendulum (a) and the standard gravitational pendulum (b). Note that in both cases, the potential energy increases with increasing z.

The potential energy $q\Phi(\theta)$ in the case of the electrostatic pendulum is given by

$$q\Phi(\theta) = \frac{qV_0 a^2}{2d^2}\cos\theta = \frac{qV_0 a^2}{2d^3} z, \tag{16}$$

where z is the vertical distance, as shown in Fig. 2. In the case of the gravitational pendulum, the potential $\Phi_g(z)$ is simply given by $\Phi_g(z) = mgz$. Thus, we can define an "equivalent gravity" for the electrostatic pendulum, g_{eff}, which is given by

$$g_{eff} = \frac{qV_0 a^2}{2md^3}. \tag{17}$$

Noting that the expression for the period of an isochronous gravitational pendulum, T, is given by

$$T = 2\pi\sqrt{\frac{d}{g}}, \tag{18}$$

the period of the lunar dust pendulum is

$$T = 2\pi\frac{d}{a}\sqrt{\frac{2md^2}{qV_0}}. \tag{19}$$

This equation establishes the scaling relationships in the model. For example, lowering the charge q on the dust grain by a factor of two will increase the period by a factor of $\sqrt{2}$.

4. Validity of assumptions: time and length scales

The calculations here use the vacuum solution for the crater potential and take the charge of the lunar dust grain as constant over the time scale of its trajectory. The first condition requires that the Debye length, which serves as a characteristic length over which potentials become electrically shielded, be larger than the characteristic scale lengths of interest, namely the crater diameter and radius of the dust grain trajectory. The second condition requires that, once liberated from the surface, the currents experienced by the dust grain will not change its potential significantly over the time scale of its motion.

It is worth pointing out that we do not address here the issue of initial ejection, that is, how the dust initially overcomes its attachment to the lunar surface to execute this periodic motion, but rather we describe its motion thereafter (a common approach among electrostatic dust transport papers [e.g., Nitter et al., 1998 and references therein]). Since van der Waals forces become increasingly more important as particle size decreases, one would not expect small particles to be preferentially released from

the lunar surface. Nevertheless, various mechanisms have been proposed to release the particles from the surface including incoming micrometeorites disrupting the lunar surface layer and ejecting material (Singer and Walker, 1962) and electrostatic forces (Rennilson and Criswell, 1974). In the case of micrometeorites, dust may be lofted through comminution and high charge levels on individual grains effected through the impact process. Of course, in this case there may also be an initial velocity at the surface. However, the plasma cloud generated by the initial impact would tend to charge the dust grains negative (Horanyi et al., 2009), while the dust grains considered here, and typically in other levitation models [e.g., Colwell et al., 2005] are positively charged. In general, though, because there are a large number of dust grains on the lunar surface, only a small fraction of the dust needs participate in this process for it to be an important transport mechanism.

Furthermore, the claim that lunar electric fields are not strong enough to loft dust usually results from estimates that implicitly assume the lunar surface is perfectly smooth. Roughness on the lunar surface will create enhancements in the electric field with particularly strong electric fields occurring at corners [e.g., Hartzell et al., 2012]. So, it is likely that initial dust lofting occurs preferentially near sharp irregularities on the rough lunar regolith.

More recently, Glenar et al. (2011) have speculated that a saltation-like mechanism could be ejecting and transporting exospheric dust. They suggest that this process is initiated by meteoritic impact-generated ejecta returning to the surface at speeds below the escape velocity (i.e., the component not lost from the Moon). If the returning ejecta have enough energy to overcome the cohesive forces between dust grains on the lunar surface, then they will eject more dust and/or bounce back into the exosphere. This process is anticipated to cascade in such a way that the average energy of the dust grains tends to decrease while their abundance increases, but only if they still have sufficient energy to continue liberating dust from the surface. It is possible that slow-moving dust grains produced by this process could be either levitated and/or execute the pendulum-like motion described here, before finally being lost to the surface. Furthermore, this saltation process would also tribocharge the dust grains producing the oscillatory motion.

The first assumption of the model is that the Debye length is larger than the characteristic scale lengths of interest. The Debye length, λ, is given by

$$\lambda = \sqrt{\frac{\epsilon_0 \cdot k_b T_e}{n_0 e^2}}, \tag{20}$$

where ϵ_0 is the permittivity of free-space, 8.85×10^{-12} $C^2/N\,m^2$, $k_b T_e$ is the product of Boltzmann's constant and the plasma electron temperature, taken to be 10–12 eV, n_0 is the ambient plasma density, about 5–10 cm^{-3}, and e is the charge of an electron. These are typical solar wind electron distribution parameters, and the electrons can gain access to shadowed regions because of their large thermal speed and near-isotropic velocity distributions. Because of the assumed proximity to the terminator and/or local topographic effects, the Debye length is taken to be greater than the length scales of interest, so that we may use the vacuum solution. Note that given the values above and with reference to the example to be discussed in Section 4.2, "Typical Numbers," lunar surface Debye lengths ~10 m occur near the terminator [e.g., Stubbs et al., 2006; Farrell et al., 2007, 2010], so it is not too difficult to conceive of locations on the diverse lunar surface where the vacuum solution is valid even at these scales with a Debye length in excess of 20 m. Debye lengths are expected to be particularly large at the sunset terminator (Stubbs et al., 2010) where all observations of near-surface lunar horizon glow were made by the Surveyor landers (Rennilson and Criswell, 1974).

Additionally, one of our assumptions is that the charge on the dust grain after it leaves the surface remains constant over the time scale of its trajectory, which in the case to be discussed in the next section is ~10 s. We can estimate a lower limit for the time scale τ for the change in charge of a lunar dust grain with charge q using

$$\tau \sim \frac{q}{I}. \tag{21}$$

We use a nominal area current density of 10^{-10} A/cm^2 intended to represent all sources of current including local plasma electrons (Collier et al., 2011a; Whipple, 1981). Using this value, we estimate the current I to a dust grain of size (i.e., radius) $a_g = 0.1 \times 10^{-6}$ m, to be

$$I \sim 10^{-10}\mathrm{A/cm^2} \cdot \pi (0.1 \times 10^{-4}\mathrm{cm})^2 = 3 \times 10^{-20}\mathrm{A}. \tag{22}$$

If we take the dust to be spherical, assume a nominal 10 Volt charge, a capacitance $C = 4\pi\epsilon_0 a_g$, and note that the charge on the grain is simply given by $q = CV$, we get

$$\begin{aligned} q &= 4\pi\epsilon_0 a_g \cdot (10V) \\ &= 4\pi \cdot 8.85 \times 10^{-12}\mathrm{F/m} \cdot 0.1 \times 10^{-6}\mathrm{m} \cdot 10V \\ &= 1.1 \times 10^{-16}\ \text{coulombs}, \end{aligned} \tag{23}$$

or the equivalent of about 700 electron charges. Thus, we get a time scale τ of

$$\tau \sim \frac{10^{-16}}{3 \times 10^{-20}} \sim 3000\mathrm{s} \tag{24}$$

This is a couple orders of magnitude larger than the oscillation period, ~10 s, for a dust grain of this size given the assumed parameters. So, to a good approximation, the dust grain's charge remains constant over its orbit. Furthermore, the calculation above provides a lower limit for two reasons: (1) The actual current I that should be used in Eq. (21) is the difference between the currents into (i.e., photoelectron current and solar wind proton current) and out of (solar wind electron current) the dust grain rather than just the characteristic magnitude of the currents. Furthermore, a significant component of the plasma

electrons will be repelled before reaching the grain near the surface. These effects will of course increase τ. (2) The charge q, taken to be about 700 electrons, is based on estimating the capacitance of lunar dust as a sphere. In fact, lunar dust more closely resembles a fractal structure (Marshall et al., 2011) which can increase the capacitance dramatically (Collier et al., 2011b; Kempf et al., 2004). At fixed voltage, this in turn will increase q, increasing the time scale τ (for a given dust grain volume, a spherical shape has the lowest capacitance). Recent work by Stubbs et al. (2011) on the "dust-electron" model for the lunar ionosphere also suggests a larger capacitance for lunar grains than one might infer based on a spherical model.

It is also instructive to note how large a dust grain would need to be given values of $d = 20$ m, $a = 10$ m, $V = 10$ Volts and $V_0 = -100$ Volts to have a charging time at 10^{-6} A/m^2 of half the period. Because the charge $q = 1.1 \times 10^{-9} a_g$ and the period $T = 1.1 \times 10^{8} a_g$, the grain size satisfying this condition is 2.5×10^{-6} m, over an order of magnitude larger than the grain size in the example and on the upper end of grain sizes generally considered in levitation and transport models [e.g., Murphy and Vondrak, 1993].

4.1. The accuracy of the approximation

There are two factors that impact the accuracy, and hence the applicability, of the proposed model and analysis. First is the degree to which the dipole approximation represents the true field configuration for the idealized geometry, namely the disk embedded in a ground plane. Second and likely more important is the degree to which the idealized geometry is applicable to actual physical situations, that is the degree of generality or "robustness" of the model including how more realistically modeled topography will affect the trajectories.

With regard to the first issue, one can gain a sense of the accuracy with which the dipole approximates the actual potential configuration by noting that the field configuration can be solved analytically along the axis $\rho = 0$:

$$\Phi(\rho = 0, z) = V_0 \left[1 - \frac{z}{\sqrt{a^2 + z^2}} \right]. \tag{25}$$

By comparing this to the dipole approximation for Φ/V_0, namely $1/2(z/a)^2$, the dipole approximation appears to be accurate to within 20% even as close as two crater radii from the origin.

To investigate how "robust" the model is to boundary conditions and actual topography, we have performed numerical simulations discussed in Sections 5 and 6.

4.2. Typical numbers

There is a region on the lunar dayside with near-zero surface potential at the transition between the photoemission dominated regime (positive) and the plasma electron dominated regime (negative). This region is sometimes referred to as the "Dead Zone" and typically occurs at solar zenith angles of between about 60° and 90°, depending on the conditions (Stubbs et al., 2006; Stubbs et al., 2007). Within a small region, a degree or two, of 90° solar zenith angle (SZA), the vertical field assuming no topographic effects could get as high as -3 V/m (Stubbs et al., 2007 predict -4 V/m using LP data) which would inhibit the motion of positively charged dust. However, as shown in Farrell et al. (2007), Fig. 3, topographic effects (i.e., slopes) will cause the regions near craters at the terminator to become positively charged.

Even if the lunar surface is a few volts positive, this is small relative to the potential difference between the surface and the crater. The essential point is that there exists a relative potential difference of V_0 between the lunar surface and the disk representing the crater, and the dust assumes the potential of the surface. However, the dust could, in principle, become charged independent of the surface potential by other means.

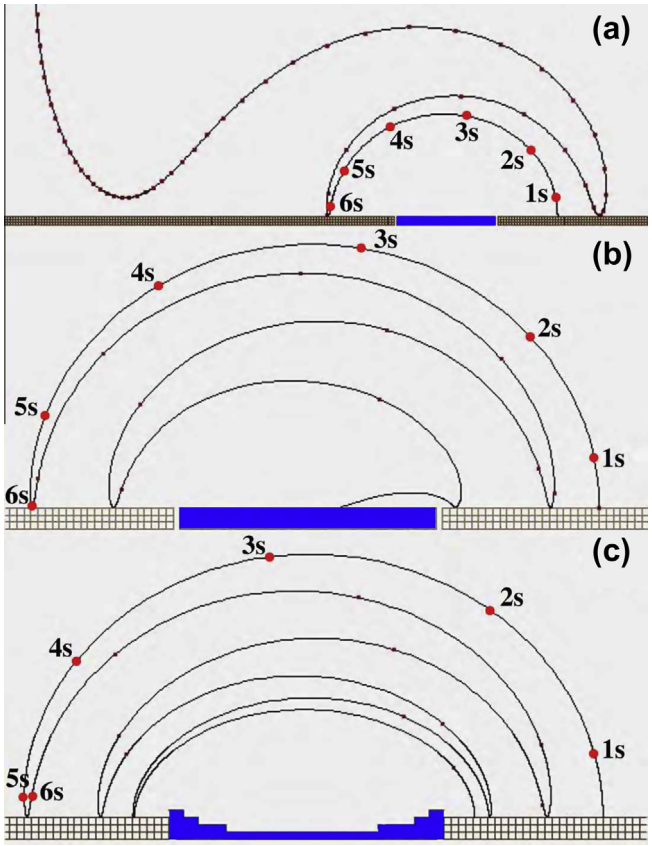

Fig. 3. Particle trajectories given the parameters from Section 4.2, "Typical Numbers," from a Simion simulation. The labels indicate time in seconds so that the half-period of oscillation, that is the time it takes the dust grain to jump over the crater, is close to the ~6 s predicted by the analysis. The top panel (a) shows a Simion simulation with a disk of 20 gu radius at the center of a grounded disk of radius 223 gu. The middle panel (b) shows a Simion simulation with a disk of 20 gu radius at the center of a grounded plane surrounded by a grounded sphere of radius 223 gu. The bottom panel (c) shows a Simion simulation of a crater of 20 gu radius that has an elevated rim and goes below the ground plane at the center of a grounded sphere of radius 223 gu.

Assuming a Debye length of greater than about 20 m, we consider distances only less than about 20 m and take the vacuum solution to be a reasonable approximation to the field configuration. We consider a small spherical dust grain of radius $a_g = 0.1 \times 10^{-6}$ m $= 10^{-7}$ m selected based on lunar horizon glow observations (Zook and McCoy, 1991; Glenar et al., 2011; McCoy, 1976). Assuming a mass density of 2700 kg/m^3 (a nominal value for the mass density of lunar dust), this amounts to a mass, m, of

$$m = 2700\text{kg/m}^3 \cdot \frac{4\pi}{3}(10^{-7}\text{m})^3 = 1.1 \times 10^{-17}\text{kg} = 6.6 \times 10^9\text{amu}. \quad (26)$$

We assume a crater with a radius of 10 m with a potential of −100 V. We assume further that the dust particle is at a distance of 20 m from the crater center and that the dust has charge on it equivalent to a sphere at +10 V. As discussed earlier, the charge on such a grain is 1.1×10^{-16} coulombs or about 700 electrons.

A grain potential of +10 Volts is chosen only as a nominal value for illustration because it is typical of the lunar surface potentials actually observed on the Moon by SIDE [e.g., Collier et al., 2011a and references therein]. Furthermore, the charge determined above assumes a dust grain with spherical geometry and non-spherical or fractal geometry can easily increase the charge corresponding to a given potential by at least a factor of two (Collier et al., 2011b; Stubbs et al., 2011). The effect of assuming a different charge is easily calculated. Referring to Eq. (19), the effect of assuming +5 Volts, for example, would be simply to increase the period by a factor of $\sqrt{2}$. The circular motion would still, of course, be maintained.

In this analysis, we have ignored gravity in comparison to electrostatic forces. To check this, we compare the electrostatic acceleration $a_p = F_p/m$ where

$$\frac{F_p}{m} \sim \frac{(100\text{Volts}) \cdot (10\text{m})^2 \cdot 1.1 \times 10^{-16}\text{coul}}{(20\text{m})^3 \cdot 1.1 \times 10^{-17}\text{kg}} = 12.7\text{m/s}^2, \quad (27)$$

to the gravitational acceleration $a_{grav} = -g_{moon} = -1.6$ m/s^2. So, clearly the electrostatic forces dominate. However, the gravitational acceleration is of the order of 10% of the electrostatic acceleration and will have a perturbing effect on the dust grain trajectories. Of course, gravitational perturbations will become increasingly more important for larger grains and smaller potentials.

5. Simulations

We have performed Simion 8.0 (http://simion.com) numerical simulations using the specific parameters given in the previous section. Simion 8.0 is a commercially available software package that solves Laplace's equation subject to specific boundary conditions using the relaxation method. Simion 8.0 allows the user to trace charged particle trajectories through the resultant potential configuration (and repeated runs give the same results). Because Simion 8.0 uses a finite-sized grid, it cannot handle boundary conditions at infinity and so cannot perfectly reproduce the physical situation described here. Nevertheless, it provides a good approximation.

The total dust grain energy in the Simion simulations, which should remain zero throughout the dust grain's trajectory, can become as high as a few eV over the trajectory. This is in comparison to typical potential energies of the dust grain in the negative keV range and, conversely, typical kinetic energies in the positive keV range. Insofar as the total grain energy does not stay at zero, this is certainly a result of numerical errors on the grain trajectory as well as grid resolution and boundary condition limitations. However, energy is conserved remarkably well as the agreement between model and simulations will show.

Using Eq. (19) and the numbers from the previous section, namely $m = 1.1 \times 10^{-17}$ kg, $d = 20$ m, $a = 10$ m, $q = 1.1 \times 10^{-16}$ coulombs, and $V_0 = -100$ Volts, we get

$$T = 2\pi \frac{d}{a}\sqrt{\frac{2md^2}{qV_0}} = 11.2\text{s}. \quad (28)$$

So, in about 6 s (correcting for large amplitude oscillation), a 0.1×10^{-6} m dust grain charged to +10 V at a distance of 20 m from the center of a 10 m radius crater charged to −100 Volts will jump to the other side of the crater. It will then jump back again in an oscillatory motion.

The three panels of Fig. 3 show the results of Simion simulations using 500 mm/gu (gu is a Simion "grid unit"), −100 Volt potential on the center disk, a mass of 6.6×10^9 amu, a positive charge equal to q = 688e$^-$, a central disk radius of a = 20 gu·0.5 m/gu = 10 m, a start position of (0,40) gu = (0,20) m, and markers at one second intervals.

The dust grain does undergo oscillatory motion with a jump time of about six seconds in all cases and repeats that motion for at least three jumps. To address the effect of a finite-sized simulation volume that does not allow setting the potential to zero at infinity, we compared two approaches to the outside boundary conditions. Both of these cases simulate a disk of radius 20 grid units centered in a ground plane of radius 223 grid units.

The top panel (a) shows the simulated trajectory with no other boundary conditions. Here, the grain leaves the simulation area after about three jumps across the crater. The center panel (b) by comparison shows the simulated trajectory if the potential is forced to zero on a sphere of radius 223 grid units. Here the particle jumps the crater four times and eventually lands inside the crater. In both cases, the trajectory demonstrates oscillatory behavior showing that the results are robust with respect to how far-away boundary conditions are handled.

Because the oscillatory motion is unstable, it is not surprising that the dust grain does not remain in circular motion indefinitely, probably because of the limitation in a finite mesh, as used by Simion, to perfectly handle the

boundary conditions and/or because of the neglected higher order terms in the multipole expansion. However, because the motion is unstable, one model prediction is that dust grains near charged craters will tend to either be ejected from their vicinity, as in the simulation in panel (a), or converge into and become trapped inside the crater as in panel (b), depending on the nature of the perturbation. The latter leads to a "dust ponding" phenomenon (Veverka et al., 2001; Robinson et al., 2001) similar to that described by Colwell et al. (2005) albeit through a different physical mechanism in this case.

In the bottom panel (c), a more realistic crater topography was employed with a small elevated rim and a crater floor below the ground plane with the upper boundary condition as in panel (b). In this scenario, the dust grain still oscillates and moves closer to the crater with each jump, much like panel (b).

Simion follows the dust grain trajectories until they hit a surface (in Simion parlance, the particles "splat" when they hit an "electrode"). In Fig. 3 panel (b), the trajectory stops because the dust grain has hit the crater floor. In Fig. 3 panel (c), because the dust grain starts out just above the ground plane at rest, small numerical errors eventually take it below the surface and cause the simulation to stop.

As Fig. 3 panel (b) illustrates, we have not included in the model any possible effects, such as sticking, that may occur if the dust grain gets close to the surface. Of course, if the dust grain sticks, it will only hop once over the crater. However, as will be shown later, one effect of perturbations is that the closest approach of the trajectories moves farther away from the surface. Note that this also implies that the perturbation due to gravity will not necessarily cause the dust grains to hit the surface after traversing the crater only one time.

Finally, as discussed in Section 3, "Analytical Solution," the dominant term at a distance given any arbitrarily shaped charged crater will be the dipole term, so the oscillatory behavior occurs even for irregular-shaped craters or, equivalently, for charging that is not uniform across the crater floor.

To illustrate, one might expect only the side of the crater closest to the sun will be most effectively shaded and produce a negative potential while the opposite side is exposed to some sunlight and is close to zero potential [e.g., Farrell et al., 2007, Fig. 3; Stubbs et al., 2010]. To simulate this, we have taken the crater model above with the same parameters and set a circular region of radius 5 m at the back to zero potential to generate a non-circularly symmetric crescent profile. Fig. 4 shows the dust trajectories around the crater which still exhibit oscillatory behavior.

To verify the scaling relationship, Eq. (19), we have performed simulations varying the parameters a, d, m, q, and V_0, and the oscillatory behavior persists in those simulations, as well. So, this oscillatory behavior appears robust to variations in the idealized model of a disk in an infinite ground plane.

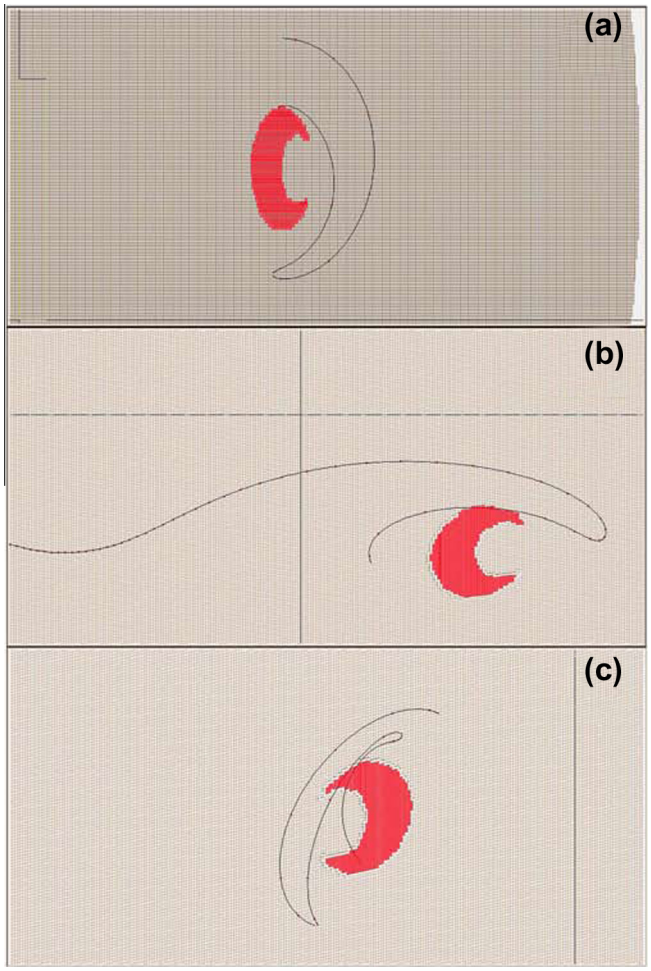

Fig. 4. Simulations showing the dust trajectories over a non-circularly symmetric crater. Panels (a), (b), and (c) show three different runs for longitudinal, transverse, and diagonal trajectories.

6. Effect of Debye shielding

As discussed previously, perturbations to the dipole potential will cause the dust grain trajectories to be ejected from the crater vicinity (perhaps becoming ballistic dust similar to that observed by LEAM or lofted grains similar to the dust fountain model of Stubbs et al., 2006), or cause the dust grain trajectories to end up in the craters contributing to dust ponding.

One perturbation effect that will always be present is the effect of Debye shielding of the vacuum potential solution by the ambient plasma. This effect may be modeled by modifying the potential given in Eq. (11) to include a shielding term:

$$\Phi(r,\theta) = \frac{V_0 a^2}{2} \cdot \frac{\cos\theta}{r^2} \cdot \exp\left\{-\frac{r}{\lambda}\right\}. \tag{29}$$

where λ is the Debye length or shielding distance.

Interestingly, for small ωt (where $\omega T = 2\pi$) and r_0/λ, the perturbation, r_1, to the radius r_0 goes as

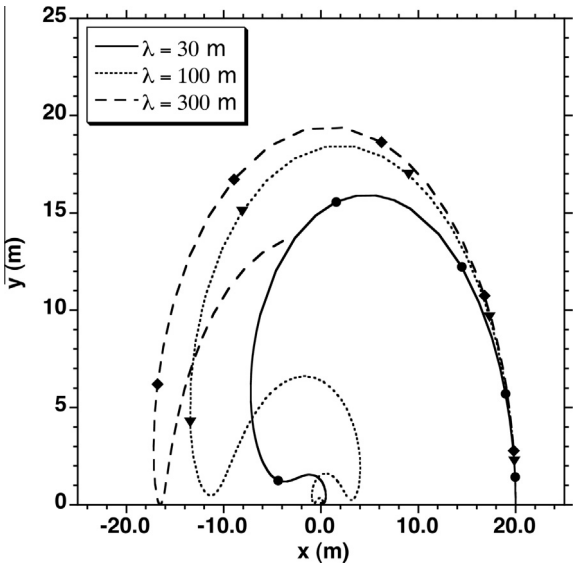

Fig. 5. Dust trajectories in a dipolar field with Debye shielding using the previous parameters. The dipole is at $x = 0,\ y = 0$. The trajectories are plotted for Debye lengths of 30, 100, and 300 m with the symbols at one second intervals. Even when the Debye length is comparable to the other scale lengths, the dust grains exhibit the pendulum-like behavior.

$$r_1(t) \approx -\frac{r_0^2}{\lambda}\frac{(\omega t)^4}{24}. \tag{30}$$

Thus, the effect of Debye shielding will always be to initially decrease the radius. Because the equilibrium trajectory is unstable, Debye shielding will result in the dust grain eventually becoming deposited into the crater.

To illustrate this point, Fig. 5 shows the dust grain trajectories in a dipole field for the values from Section 4.2 for three different Debye shielding lengths, 30, 100, and 300 m. In every case, the oscillatory behavior is present with a half-period a bit over 5 s, and the trajectories move progressively closer with time to the center, more quickly at smaller λ.

7. Discussion

The results of the model presented here are qualitatively similar to those of Colwell et al. (2005) insofar as they predict vertical and horizontal dust motion that results in oscillatory behavior that deposits grains into shadowed regions. However, the models are remarkably different in many key ways, for example: (i) ambient environment: Colwell et al. assume a photoelectron layer while we assume a vacuum field with Debye shielding, (ii) location: Colwell et al. assume a dayside surface while we assume near-terminator topographic shadows, (iii) Debye length: Colwell et al. assume a crater larger than the Debye length while we assume a Debye length larger than the crater, (iv) body: Colwell et al. assume an asteroid while we assume the Moon, but both have broader application to other airless bodies, (v) approach: Colwell et al. present a numerical model while we perform an analytic calculation supported by simulations, (vi) Colwell et al. include gravity while we assume (and show) that gravity is negligible compared to electrostatic forces, and perhaps most importantly (vii) Colwell et al. ignore horizontal electric fields while we include them in a self-consistent manner as an intrinsic and necessary aspect of the model. Perhaps the similar qualitative behavior of the two models suggests that oscillatory dust transport, and the "swarming" of dust over shadowed regions, is a general feature of airless bodies.

Because the model predicts oscillatory motion across the crater, it also shows that dust may be transported horizontally on the lunar surface yet not travel great distances. Thus, the fact that young, light-colored surface features on the moon persist for extended periods of time does not preclude the presence of substantial dust transport both vertically and horizontally. The dust may simply not travel very far.

Although the model proposed here is idealized to allow an analytic treatment, we anticipate that more realistic numerical models of dust transport will also show this qualitative behavior – that is certain dust populations "jumping" back and forth across locally charged craters and other topographic structures. There may, in fact, be evidence for such a canopy of pendulum-type dust in the Surveyor images, for example, Fig. 1 of Rennilson and Criswell (1974).

As an example of the frequent occurrence of this oscillatory behavior, Poppe et al. (2012) in their Fig. 6 show the results of a two-dimensional dust tracing code where individual dust grains are introduced into a particle-in-cell-modeled plasma environment. Their Fig. 6 panels (b) and (c) shows that after about 45 s the horizontal and vertical velocities of the particles execute oscillatory motion with a period of about 7–14 s. Although the simulation applies to the subsolar point with the potential V_0 of the 7 m diameter crater about −3 Volts with respect to the surrounding surface exterior to the crater (their Fig. 1), we apply Eq. (19) and compare to Poppe et al.'s simulated period. They use a dust grain of 24 nm radius, which with their assumed density of 2500 kg/m^3 gives a mass m = 1.4×10^{-19} kg. The particle starts oscillating at about the crater's edge, so $d = a = 3.5$ m, and over the period of oscillation has a

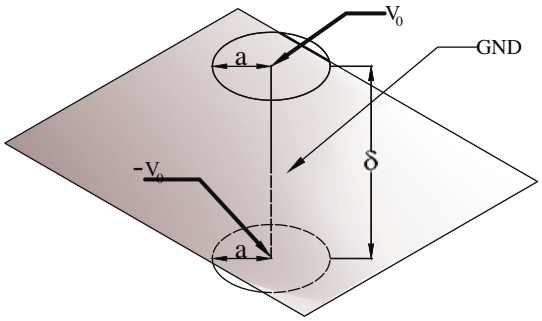

Fig. 6. The dipole moment $V_0 a^2/2$ may be deduced by considering two disks of radius a and potentials V_0 and $-V_0$ spaced a small distance δ apart. By symmetry, the plane between them is at zero potential.

charge $q = 3.2 \times 10^{-19}$ coulombs. Thus, Eq. (19) gives a period T = 12 s, roughly in agreement with Poppe et al.'s simulated period and further evidence of the wide applicability of the analytic model presented here.

8. Conclusions

The behavior of charged dust on the lunar and other surfaces is currently an active area or research. Future missions such as the Lunar Atmosphere and Dust Environment Explorer (LADEE), currently to be launched in May 2013 (Elphic et al., 2011), assure that this area will continue to remain vibrant over the next few years.

Current evidence and models indicate that transported dust will be deposited into shadowed regions on airless bodies [e.g., Colwell et al., 2005]. The model presented here assumes only basic conditions that are believed to exist on airless bodies: namely charged dust in the presence of differential charging from topographic effects such as those illustrated in Fig. 3 of Farrell et al. (2007).

Simulations show that the analytic model results are very robust and insensitive to perturbations such as crater shape and the presence of Debye shielding. The analytical treatment predicts both horizontal and vertical dust motion resulting in "swarms" of dust above craters (dust grains hopping over craters) some of which will become deposited into the crater. The simple physical conditions required by the model predict that horizontal and vertical dust transport are fundamental properties of airless bodies.

This effect would preferentially occur at sunset due to the offset between the optical shadow and the plasma wake (Stubbs et al., 2010). At this location the surface is exposed to a very tenuous plasma and sunlight simultaneously, which gives a larger Debye length than at sunrise, and could produce an ~0 V surface with negatively charged craters. Although we have considered the motion of a single dust grain, there will be many dust grains following this oscillatory motion resulting in dust "canopies" or "swarms" over shadowed craters at certain locations on the lunar surface, perhaps observed by the Surveyors as lunar horizon glow (Rennilson and Criswell, 1974).

9. Appendix

There is the following heuristic argument for determining the dipole moment of a disk in a plane. We can approximate the physical situation shown in Fig. 1 by using two disks, one at potential V_0 and one at potential $-V_0$ separated by a small distance δ along the z-axis such that V_0 is above the origin by $\delta/2$ and $-V_0$ is below the origin at $z = -\delta/2$, as shown in Fig. 6. The symmetry in this problem assures that the plane $z = 0$ is at ground, so that taking δ to be very small, we approximate, in the half-space region $z > 0$, the modeled physical configuration with a ground plane at $z = 0$ and $\rho > a$ and the disk of radius a around the origin held at V_0. If δ is small relative to the radius, the two disks form a parallel plate capacitor with a capacitance C given by

$$C = \frac{A}{4\pi \cdot k \cdot d}, \tag{31}$$

where $k = 1/4\pi\epsilon_0 = 9 \times 10^9\ \mathrm{N m^2/coul^2}$, $A = \pi a^2$ is the area of the plates, and d is the distance between the plates, δ. Substituting this into Eq. (31) yields

$$C = \frac{a^2}{4k\delta}. \tag{32}$$

Since

$$Q = C \cdot \Delta V = 2CV_0, \tag{33}$$

and the dipole moment $p = Q \cdot \delta$

$$p = 2CV_0\delta = \frac{V_0 a^2}{2k}, \tag{34}$$

so that in the multipole expansion of the potential, the dipole term is $V_0 a^2/2$.

Acknowledgments

This work was supported through the Dynamic Response of the Environment At the Moon (DREAM) NASA Lunar Science Institute team and NASA Grant NNX08AN76G (LROPS) as well as by NASA LASER 132438.01.15.01.06 issued through the Science Mission Directorate/Planetary Science Division and Exploration Systems Mission Directorate/Advanced Capabilities Division. Special thanks to Greg Delory for pointing out relevant references and to Dennis Chornay and John Keller for helpful discussions.

References

Abramowitz, M., Stegun, I.A.. Handbook of Mathematical Functions with Formulas, Graphs, and Mathematical Tables. Dover Publications Inc., New York, 1972.

Berg, O.E., Wolf, H., Rhee, J.W. Lunar soil movement registered by the Apollo 17 cosmic dust experiment, in: Elsässer, H., Fechtig, H. (Eds.), Interplanetary Dust and Zodiacal Light. Springer-Verlag, Berlin, pp. 233–237, 1976.

Borisov, N., Mall, U. Charging and motion of dust grains near the terminator of the moon. Planet. Space Sci. 54, 572–580, 2006.

Collier, M.R., Hills, H.K., Stubbs, T.J., Halekas, J.S., Delory, G.T., Espley, J., Farrell, W.M., Freeman, J.W., Vondrak, R. Lunar surface electric potential changes associated with traversals through the Earth's foreshock. Planet. Space Sci. 59 (14), 1727–1743, http://dx.doi.org/10.1016/j.pss.2010.12.010, 2011a.

Collier, M.R., Stubbs, T.J., Keller, J.W., Farrell, W.M., Marshall, J., Richard, D.T. A fractal model for the capacitance of lunar dust and lunar dust aggregates. NASA Lunar Science Forum Abstract. Ames Research Center, 2011b.

Colwell, Joshua E., Gulbis Amanda, A.S., Horányi, Mihály, Robertson, Scott Dust transport in photoelectron layers and the formation of dust ponds on Eros. Icarus 175, 159–169, 2005.

Colwell, J.E., Batiste, S., Horanyi, M., Robertson, S., Sture, Steve Lunar surface: dust dynamics and regolith mechanics. Rev. Geophys. 45 (2), RG2006, 2007.

Elphic, Richard, Delory, G., Colaprete, A., Horanyi, M., Mahaffy, P., Hine, B., Harris, D., Salute, J., Grayzeck, E., Boroson, D. Status of

NASA's lunar atmosphere and dust environment explorer (LADEE). NASA Lunar Science Forum. Ames, California, 2011.

Farrell, W.M., Stubbs, T.J., Vondrak, R.R., Delory, G.T., Halekas, J.S. Complex electric fields near the terminator: the near-surface wake and accelerated dust. Geophys. Res. Lett. 34, L14201, http://dx.doi.org/10.1029/2007GL029312, 2007.

Farrell, W.M., Stubbs, T.J., Delory, G.T., Vondrak, R.R., Collier, M.R., Halekas, J.S., Lin, R.P. Concerning the dissipation of electrically charged objects in the shadowed lunar polar regions. Geophys. Res. Lett. 35, L19104, http://dx.doi.org/10.1029/2008GL034785, 2008.

Farrell, W.M., Stubbs, T.J., Halekas, J.S., Killen, R.M., Delory, G.T., Collier, M.R., Vondrak, R.R. Anticipated electrical environment within permanently shadowed lunar craters. J. Geophys. Res. 115, E03004, http://dx.doi.org/10.1029/2009JE003464, 2010.

Fenner, M.A., Freeman Jr., J.W., Hills, H.K. The electric potential of the lunar surface. Geochim. Cosmochim. Acta 3, 2877–2887, 1973.

Glenar, D.A., Stubbs, T.J., McCoy, J.E., Vondrak, R.R. A reanalysis of the Apollo light scattering observations and implications for lunar exospheric dust. Planet. Space Sci. 59 (14), 1695–1707, http://dx.doi.org/10.1016/j.pss.2010.12.003, 2011.

Hartzell, Christine, Wang, Xu, Scheeres, Daniel, Horanyi, Mihaly. Experimental demonstration of the importance of cohesion in electrostatic dust lofting. NASA Lunar Science Forum Abstract. Ames Research Center, 2012.

Horanyi, M., Munsat, T., Robertson, S.H., Sternovsky, Z., Wang, X. Impact generated plasmas on the lunar surface. EOS Trans. AGU, 90, 52, Fall Meeting Suppl., P32A-04, 2009.

Hörz, F., Grieve, Richard, Heiken, Grant, Spudis, Paul, Binder, Alan. Lunar surface processes, in: Lunar Source Book: A User's Guide to the Moon. Cambridge University Press, pp. 61–120, 1991.

Jackson, J.D. Classical Electrodynamics, second ed John Wiley and Sons Inc., New York, 1975.

Nitter, T., Havnes, O., Melanso, F. Levitation and dynamics of charged dust in the photoelectron sheath above surfaces in space. J. Geophys. Res. 103, 6605–6620, 1998.

Kempf, S., Srama, R., Altobelli, N., Auer, S., Tschernjawski, V., Bradley, J., Burton, M.E., Helfert, S., Johnson, T.V., Krüger, H., Moragas-Klostermeyer, G., Grün, E. Cassini between earth and asteroid belt: first in-situ charge measurements of interplanetary grains. Icarus 171, 317–335, 2004.

Manka, R.H. Plasma and potential at the lunar surface, in: Grard, R.J.L. (Ed.), Photon and Particle Interactions with Surfaces in Space. D. Reidel, Dordrecht, Netherlands, pp. 347–361, 1973.

Marshall, J., Richard, D., Davis, S. Electrical stress and strain in lunar regolith simulants. Planet. Space Sci. 59, 1744–1748, http://dx.doi.org/10.1016/j.pss.2010.11.005, 2011.

McCoy, J.E. Photometric studies of light scattering above the lunar terminator from Apollo solar corona photography. In: Proceedings of the Seventh Lunar Science Conference, pp. 1087–1112, 1976.

Mendis, D.A., Hill, Jay Roderick, Houpis, Harry L.F., Whipple Jr., E.C. On the electrostatic charging of the cometary nucleus. Astrophys. J. 249, 787–797, 1981.

Murphy, D.L., Vondrak, R.R. Effects of levitated dust on astronomical observations from the lunar surface. Proc. Lunar Planet. Sci. Conf. 24, 1033–1034, 1993.

Jones, Randall S. Circular motion of a charged particle in an electric dipole field. Am. J. Phys. 63 (11), 1042–1043, 1995.

O'Brien, Brian J. Review of measurements of dust movements on the moon during Apollo. Planet. Space Sci. 59 (14), 1708–1726, http://dx.doi.org/10.1016/j.pss.2011.04.016, 2011.

Poppe, A., Horányi, M. Simulations of the photoelectron sheath and dust levitation on the lunar surface. J. Geophys. Res. 115, A08106, http://dx.doi.org/10.1029/2010JA015286, 2010.

Poppe, A., Halekas, J.S., Horányi, M. Negative potentials above the dayside lunar surface in the terrestrial plasma sheet: evidence of non-monotonic potentials. Geophys. Res. Lett. 38, L02103, http://dx.doi.org/10.1029/2010GL046119, 2011.

Poppe, Andrew R., Piquette, Marcus, Likhanskii, Alexandre, Horányi, Mihály The effect of surface topography on the lunar photoelectron sheath and electrostatic dust transport. Icarus 221, 135–146, http://dx.doi.org/10.1016/j.icarus.2012.07.018, 2012.

Rennilson, J.J., Criswell, D.R. Surveyor observations of lunar horizon glow. Moon 10, 121–142, 1974.

Robinson, M.S., Thomas, P.C., Veverka, J., Murchie, S., Carcich, B. The nature of ponded deposits on Eros. Nature 413, 396–400, 2001.

Sickafoose, A.A., Colwell, J.E., Horányi, M., Robertson, S. Experimental levitation of dust grains in a plasma sheath. J. Geophys. Res. 107, 1408, http://dx.doi.org/10.1029/2002JA009347, 2002.

Singer, S.F., Walker, E.H. Electrostatic dust transport on the lunar surface. Icarus 1 (2), 112–120, 1962.

Stubbs, Timothy J., Vondrak, Richard R., Farrell William, M. A dynamic fountain model for lunar dust. Adv. Space Res. 37, 59–66, 2006.

Stubbs, T.J., Halekas, J.S., Farrell, W.M., Vondrak, R.R., in: Krüuger, H., Graps, A.L. (Eds.), Lunar Surface Charging: A Global Perspective Using Lunar Prospector Data, in Dust in Planetary Systems, SP-643. ESA Publications, pp. 181–184, Workshop, September 26–30, 2005 in Kauai, HI, 2007.

Stubbs, Timothy J., Wang, Y., Farrell, W.M., Halekas, J.S., Vondrak, R.R., Mazarico, E., Neumann, G.A., Smith, D.E., Zuber, M.T., Torrence, M.H. Characterizing the plasma shadowing and surface charging at the Moon using LOLA topographic data: predictions for the LCROSS impact. 41st Lunar Planet Sci. Conf., 2658, 2010.

Stubbs, Timothy J., Glenar, D.A., Collier, M.R., Farrell, W.M., Halekas, J.S., Delory, G.T., Vondrak, R.R. On the role of dust in the lunar ionosphere. Planet. Space Sci. 59 (13), 1659–1664, http://dx.doi.org/10.1016/j.pss.2011.05.011, 2011.

Veverka, J., Thomas, P.C., Robinson, M. Imaging of small-scale features on 433 Eros from NEAR: evidence for a complex regolith. Science 292, 484–488, 30 colleagues, 2001.

Wang, X., Horányi, M., Robertson, S. Experiments on dust transport in plasma to investigate the origin of the lunar horizon glow. J. Geophys. Res. 114, A05103, http://dx.doi.org/10.1029/2008JA013983, 2009.

Whipple, E.C. Potentials of surfaces in space. Rep. Prog. Phys. 44, 1197–1250, 1981.

Zimmerman, M.I., Farrell, W.M., Stubbs, T.J., Halekas, J.S., Jackson, T.L. Solar wind access to lunar polar craters: feedback between surface charging and plasma expansion. Geophys. Res. Lett. 38, L19202, http://dx.doi.org/10.1029/2011GL048880, 2011.

Zook, H.A., McCoy, J.E. Large scale lunar horizon glow and a high altitude lunar dust exosphere. Geophys. Res. Lett. 18, 2117–2120, 1991.